Hyperfine-enhanced nuclear polarization in $NdGaO_3$

W. Marti, M. Medarde, S. Rosenkranz, P. Fischer, and A. Furrer
Laboratory for Neutron Scattering, Eidgenössische Technische Hochschule Zürich and Paul Scherrer Institute, CH-5232 Villigen PSI, Switzerland

C. Klemenz
Crystal Growth Group, Institute of Micro-and-Optoelectronics, Swiss Federal Institute of Technology, CH-1007 Lausanne, Switzerland
(Received 27 March 1995)

The three-dimensional magnetic ordering of the Nd^{3+} ions in $NdGaO_3$ has been studied by means of neutron powder diffraction. The transition to the antiferromagnetic state takes place at $T_N \approx 1$ K. Below this temperature, the Nd^{3+} magnetic moments are oriented along the c axis in a c_z mode. The value of the saturated magnetic moment ($\approx 1.1\mu_B$) is drastically reduced below the free ion value ($3.27\mu_B$) due to crystal-field effects. The main contribution to the Nd-Nd magnetic interaction appears to be superexchange, the classical dipole-dipole interaction being too small to account for the observed Néel temperature. Below 300 mK, we observe an additional enhancement of the magnetic reflections. The analysis of the **Q** dependence of the neutron powder-diffraction intensities allowed us to interpret this increase as due to the polarization of the nuclear moments of the ^{143}Nd and ^{145}Nd isotopes in the hyperfine field created by the Nd^{3+} electronic moments. The particular conditions which lead to the observation of this phenomenon in $NdGaO_3$ are briefly discussed.

I. INTRODUCTION

It is well known that the hyperfine field created by the electronic magnetic moments can be used to orient the nuclear spins.[1,2] Although several experimental methods can be used for the study of this phenomenon, the scattering of thermal neutrons is particularly appealing since its cross section depends on the relative orientation of the spins of the neutrons and the nuclei.

Because of its high scattering power for this process, the ^{143}Nd and ^{145}Nd isotopes are ideal candidates for the study of nuclear polarization effects. In fact, in the recent literature, they have been already observed in several Nd-based compounds as $NdPd_3$,[3] Nd_2CuO_4,[4] or $NdNiO_3$.[5] The quantitative analysis of this phenomenon in the former cases was however rather complicated. In $NdPd_3$, the reason was the incommensurate magnetic structure displayed by the Nd magnetic moments. For Nd_2CuO_4 and $NdNiO_3$, the presence of a second magnetic ion (Cu^{2+} and Ni^{3+}, respectively) introduced also additional difficulties: in $NdNiO_3$, for example, a nuclear polarization of 60% and an increase of the electronic magnetic moment of Nd^{3+} from $2\mu_B$ to $\approx 3\mu_B$ produce Rietveld refinements with identical reliability factors.

To avoid these difficulties, we decided to study the perovskite $NdGaO_3$, with only one type of magnetic ion (Nd^{3+}). The crystallographic structure of $NdGaO_3$ is nowadays well known. In a previous paper dealing with the rare-earth gallates $RGaO_3$ (R=La,Pr,Nd),[6] we reported several neutron powder-diffraction experiments showing that the three compounds are orthorhombically distorted perovskites between room temperature and 12 K. In the case of $LaGaO_3$ and $PrGaO_3$, the collective tilts of the GaO_6 octahedra correspond to those of the $GdFeO_3$-type structure, which is described by the centrosymmetric *Pbnm* space group. On the other hand, $NdGaO_3$ was described by the noncentrosymmetric $Pbn2_1$ space group, following the single-crystal x-ray diffraction study of Brusset.[7] Recent higher-resolution x-ray diffraction experiments on single-domain crystals have however shown that the true symmetry of this compound is *Pbnm*.[8] The presence of a center of symmetry has been confirmed by chemical etching, using molten KOH at 500 °C.[9]

Concerning the magnetic properties, we should mention a recent work of Bartolomé *et al.*,[10] where a sharp λ-type peak in the specific heat at 0.97 K has been interpreted as the signature of the three-dimensional (3D) magnetic ordering of the Nd^{3+} magnetic moments. From the analysis of the critical region, these authors conclude that (a) the Nd-Nd magnetic interaction should be antiferromagnetic and (b) $NdGaO_3$ is one of the best realizations of a simple cubic spin-1/2 XY model in a rare-earth system.

Due to the insulating nature of $NdGaO_3$, the most probable mechanisms for the Nd-Nd magnetic coupling are the superexchange and the classical dipole-dipole interaction. Although the latter is expected to be rather small, it cannot be neglected *a priori* because of the low magnetic ordering temperature observed in this compound. From the analysis of the specific-heat data, Bartolomé *et al.*[10] found however a dipolar contribution two orders of magnitude smaller than the one needed to explain their experimental data. The superexchange interaction is then expected to be dominant.

In this work, we have reanalyzed our previous neutron

powder-diffraction data with the proper space group. In addition, we have investigated the temperature range between 10 mK and 1.4 K in order to determine the nature of the 3D magnetic ordering observed in the specific-heat measurements. In Sec. V, the group theory analysis of the possible symmetry-allowed magnetic configurations and the determination of the magnetic structure below 0.97 K are presented. The magnetic interactions responsible for the stabilization of the observed magnetic arrangement are also briefly discussed. In Sec. VI, we present clear evidence for the existence of a substantial hyperfine-enhanced polarization of the nuclear spins of the ^{143}Nd and ^{145}Nd isotopes below 300 mK. To our knowledge, this is the first time that the presence of nuclear polarization is unambiguously established from the different **Q** dependences of the nuclear (hyperfine-enhanced) and magnetic cross section in a neutron powder-diffraction experiment.

II. EXPERIMENTAL DETAILS

About 8 g of the $NdGaO_3$ polycrystalline sample were used in the present study. The synthesis route has been already described in the previous work.[6] The neutron powder-diffraction experiments were performed at the reactor Saphir of the Paul Scherrer Institute. We used the powder diffractometer DMC,[11] whose position-sensitive detector is equipped with an oscillating radial collimator to suppress the scattering from the sample environment. Several neutron powder-diffraction patterns were recorded between 10 mK and 1.4 K in the high-intensity mode ($\lambda=1.7000$ Å, vertically focusing Ge (311) monochromator, primary Soller collimation removed, scattering angle step=0.2°). To reach temperatures down to 10 mK, we used an Oxford Instruments 200 NS ^{3}He-^{4}He dilution refrigerator. The temperature gradient between the cryogenic mixture and the sample was minimized by condensing liquid helium into the sample container (a copper cylinder of 8 mm diameter and 5 cm height). A calibrated Ge resistor and a ^{60}Co/Ge γ-ray detector were used for the control of the temperature.

The data were analyzed with the Rietveld program FULLPROF.[12] To refine the structure parameters, we reanalyzed the high-resolution neutron powder-diffraction data published in Ref. 6. The results obtained for the 12 K pattern by using the *Pbnm* space group are shown in Table I. As they are not expected to change essentially below this temperature, they were kept fixed for the refinement of the remaining low-temperature patterns. To reduce the number of free parameters, the background was described by interpolating between several selected points. A Gaussian function and the usual Caglioti formula were used to describe the profile and the full width at half maximum of the Bragg reflections, respectively. The values of the resolution parameters were refined for the 1.4 K pattern (paramagnetic) and kept fixed for the subsequent low-temperature refinements. The only free parameters were then the scale factor, the zero point of the diffractometer, the Nd magnetic moment, and the nuclear polarization (see next sections). For the difference patterns, the scale factor was fixed in accordance with the monitor counts of the subtracted data.

TABLE I. Refined structural parameters of $NdGaO_3$ at 12 K.

$NdGaO_3$, space group *Pbnm*		
a(Å)		5.4223(2)
b(Å)		5.4994(2)
c(Å)		7.6989(3)
Nd	x	0.0108(4)
	y	0.0439(3)
	z	0.25
	B(Å^2)	−0.11(3)
Ga	x	0.5
	y	0
	z	0
	B(Å^2)	0.00(3)
O(1)	x	0.9174(5)
	y	0.4803(4)
	z	0.25
	B(Å^2)	0.13(5)
O(2)	x	0.2910(3)
	y	0.2928(3)
	z	0.4558(0)
	B(Å^2)	0.12(4)
R_{wp}		7.89
$R_{\exp}$		3.44
R_{Bragg}		4.69
χ^2		5.25

III. RESULTS

Figure 1(a) shows the low-angle part of the neutron powder-diffraction pattern recorded at 1.4 K. At this temperature the sample is paramagnetic ($T_N=0.97$, see Ref. 10) and all the reflections are then purely nuclear. In Fig. 1(b) the same pattern at 300 mK is displayed. A comparison with the previous one indicates the existence of several additional reflections, all of them indexable with the crystallographic unit cell (wave vector $\mathbf{k}=\mathbf{0}$). The same situation is found in Fig. 1(c), which shows the pattern recorded at 10 mK. The only difference is an additional enhancement of the new reflections.

Figures 2(a) and 2(b) display the thermal evolution of the integrated intensities of the (010)+(100) and (012)+(102) reflections, respectively. Although their nature cannot be unambiguously established without carrying out a polarization analysis, their characteristic temperature dependence, as well as the coincidence of the onset temperature (≈ 1 K) with the anomaly observed in the specific-heat measurements (≈ 0.97 K) suggest that all of them are related with the cooperative ordering of the Nd^{3+} magnetic moments. Other experimental facts supporting this assignment are (a) the decrease of the paramagnetic background below 1 K and (b) the absence

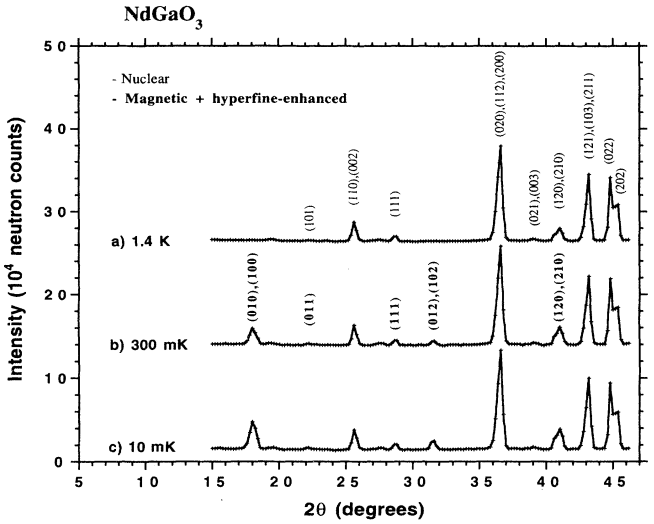

FIG. 1. Low angle part of the neutron powder-diffraction patterns of $NdGaO_3$ at 1.4 K, 300 mK, and 10 mK. The intensities have been normalized to that of the 1.4 K pattern. The counting rate was in all the cases 6250 counts/h and the measuring times 39, 8, and 45 h, respectively.

of changes in both the positions and the intensities of the purely nuclear reflections.

The enhancement of the integrated intensities observed below 300 mK is due to the polarization of the nuclear spins of the ^{143}Nd and ^{145}Nd isotopes in the hyperfine field created by the electronic Nd^{3+} magnetic moments. The reasons which lead to this conclusion will be addressed later in the discussion.

IV. THEORY

Significant polarization of the nuclear spins **I** in the hyperfine field produced by the electronic magnetic moments μ can be reached in the milliKelvin temperature range by nuclides with large enough hyperfine coupling constants A. This is the case, for example, of ^{59}Co in CoF_2 (Ref. 13) or ^{165}Ho in $HoBa_2Cu_3O_7$ (Ref. 14) and HoF_3,[15] where polarizations of 18% (Ref. 13) and 100% (Ref. 14) have been observed at ≈ 10 mK. ^{143}Nd and ^{145}Nd, which are the only Nd isotopes with nonzero nuclear spin, are also good candidates to observe this effect.[3,4] Although in natural Nd their respective abundances are only 12.18 and 8.30 %, they possess a high nuclear spin ($I=7/2$ in both cases) and quite large hyperfine constants[16] (-0.91 and -0.57 μeV for ^{143}Nd and ^{145}Nd, respectively). Another interesting characteristic of these two isotopes is that they make relatively easy the observation of the polarization effects by means of neutron diffraction. Following Glättli and Goldman,[2] the cross section for a coherent scattering process in magnetic samples containing polarized nuclei is for the case of unpolarized neutrons

$$\frac{\sigma_c}{4\pi}=b_c^2+\left|\alpha\mathbf{M}_\perp+\frac{1}{2}b_N I\mathbf{P}\right|^2 \tag{1}$$

with

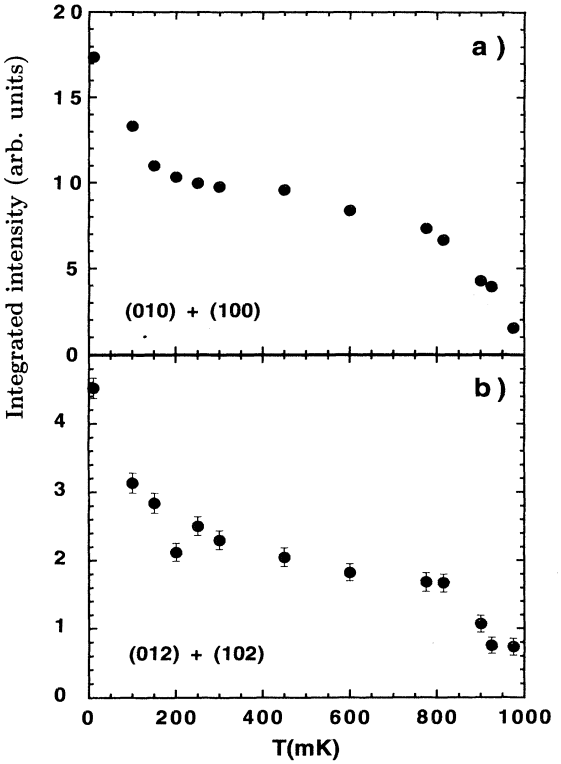

FIG. 2. Thermal evolution of the integrated intensities of some magnetic reflections: (a) (010)+(100); (b) (012)+(102). In (a) the error bars are smaller than the size of the points.

$$b_N=\frac{2b_i}{\sqrt{I(I+1)}} \quad \text{and} \quad \alpha=\frac{r_e\gamma}{2} . \tag{2}$$

Here, b_c, b_i, and α are the coherent, incoherent, and magnetic scattering lengths, respectively, **P** a unit vector in the polarization direction, r_e the classical radius of the electron, and γ the gyromagnetic ratio for the neutron. $\mathbf{M}_\perp$ is given by $\mathbf{M}_\perp=\mu_\perp f(\mathbf{Q})$ where $\mu_\perp$ is the magnetic moment component perpendicular to the scattering plane and $f(\mathbf{Q})$ is the magnetic form factor. The value of α is 2.696 fm/μ_B (the same for all the elements) and those of b_c and $1/2b_N$ for natural Nd are 7.69 and 0.92 fm, respectively. Thus, the cross sections of the three scattering processes are of the same order of magnitude. This favorable situation is due to the unusually high values of b_i for ^{143}Nd and ^{145}Nd, namely, 21.1(6) and 13(7) fm, respectively. Note also the different **Q** dependences of the three cross sections: While b_c and $1/2b_N I\mathbf{P}$ are **Q** independent, $\alpha\mathbf{M}_\perp$ decreases with Q [via $f(\mathbf{Q})$] and is zero for scattering vectors parallel to the magnetization. This property will be used in Sec. VI to probe the nuclear origin of the enhancement of the reflections below 300 mK.

From the thermodynamic point of view, the single-ion Hamiltonian which describes the ground state of the Nd^{3+} ions in $NdGaO_3$ is

$$H=H_{\text{CEF}}+H_{\text{mf}}+H_{\text{hyper}} . \tag{3}$$

Here, H_{CEF} is the crystalline-electric-field (CEF) Hamil-

tonian, H_{mf} is an effective mean-field term describing the magnetic interaction, and H_{hyper} accounts for the hyperfine coupling between the electronic and nuclear spins. The CEF Hamiltonian is most conveniently written in terms of tensor operators C_q^k:[17]

$$H_{CEF}=\sum_{k=1}^{3}\sum_{q=-k}^{k}B_q^kC_q^k \ . \tag{4}$$

The CEF parameters B_q^k are in general complex quantities, and the restriction to real potentials in (4) leads to the condition $B^k_{-q}=(-1)^q(B_q^k)^*$. Because the overall CEF splitting ($\approx$70 meV) is comparable to the intermultiplet splitting energies ($\approx$250 meV for Nd^{3+}), the usual treatment of the CEF potential as a perturbation of the ground-state multiplet $^4I_{9/2}$ alone is inappropriate. Thus, the CEF calculations have to be performed in the intermediate-coupling approximation, in which the CEF interaction is simultaneously diagonalized with the electrostatic and spin-orbit interactions defined by the Hamiltonian[17]

$$H_{el}+H_{SO}=\sum_{k=1}^{3}E^k\cdot e_k+\xi\cdot A_{SO} \ . \tag{5}$$

The matrix elements e_k and A_{SO} have been tabulated by Nielson and Koster.[18] The free-ion electrostatic and spin-orbit integrals E^k and ξ can be taken, for example, from Ref. 17.

The explicit form of the mean-field Hamiltonian H_{mf} is

$$H_{mf}=\lambda\langle m_z\rangle m_z \ , \tag{6}$$

where $\mathbf{M}=-(\mathbf{L}+2\mathbf{S})$ is the magnetic moment operator and $\langle\cdots\rangle$ stands for the thermal average. The molecular field constant λ is given by the inverse paramagnetic susceptibility of the Néel temperature, thus λ is essentially determined by the CEF parameters. Finally, the Hamiltonian for the hyperfine interaction in (3) takes the form

$$H_{hyper}=\frac{A}{g_J}\{\langle I_z\rangle m_z+I_z\langle m_z\rangle\} \ , \tag{7}$$

where I_z denotes the nuclear-spin operator and g_J is the Landé factor.

V. MAGNETIC STRUCTURE BETWEEN $T_N\approx1$ K AND 300 mK

A. Group theory analysis

The possible magnetic structures compatible with the *Pbnm* symmetry have been studied by Bertaut.[19] For $\mathbf{k}=\mathbf{0}$, the eight irreducible representations of the wave-vector group $G_{\mathbf{k}}$ (which in this case is also *Pbnm*) are one dimensional. A summary of the transformation properties for the (4*c*) Wyckoff position is displayed in Table II. In it we followed Bertaut's notation for the basis functions, that is

$$\begin{aligned}\mathbf{f}&=\mathbf{s}_1+\mathbf{s}_2+\mathbf{s}_3+\mathbf{s}_4 \ ,\\ \mathbf{a}&=\mathbf{s}_1-\mathbf{s}_2-\mathbf{s}_3+\mathbf{s}_4 \ ,\\ \mathbf{g}&=\mathbf{s}_1-\mathbf{s}_2+\mathbf{s}_3-\mathbf{s}_4 \ ,\\ \mathbf{c}&=\mathbf{s}_1+\mathbf{s}_2-\mathbf{s}_3-\mathbf{s}_4 \ ,\end{aligned} \tag{8}$$

TABLE II. Magnetic modes and Shubnikov groups for the Nd sites (4*c* Wyckoff position) in the space group *Pbnm*. The irreducible representation *j* is labeled by the symbol Γ_j. The subscript *g*/*u* (gerade/ungerade) indicates the character $+1/-1$ of the inversion center $\bar{1}$ and the + and − symbols those of the space group generators 2_{1x},2_{1y}, respectively. Here, the notation 2_{1x},2_{1y} and $\bar{1}$ stands for the two binary screw axes at $(x,1/4,0)$ and $(1/4,y,1/4)$ and the inversion center at (1/2,0,0). If a magnetic structure can be described, for instance, by the (g_xa_y-) mode, the four Nd atoms in the unit cell will show the following magnetic moments: $Nd_1(\mu_x,\mu_y,0)$; $Nd_2(-\mu_x,-\mu_y,0)$; $Nd_3(\mu_x,-\mu_y,0)$; $Nd_4(-\mu_x,\mu_y,0)$.

Nd(4*c*) in *Pbnm* $\{2_{1x},2_{1y}\}$	*x*	*y*	*z*	Shubnikov group
$\Gamma_{1g}(++)$			c_z	*Pbnm*
$\Gamma_{2g}(+-)$	f_x	c_y		*Pbn'm'*
$\Gamma_{3g}(-+)$	c_x	f_y		*Pb'nm'*
$\Gamma_{4g}(--)$			f_z	*Pb'n'm*
$\Gamma_{1u}(++)$	g_x	a_y		*Pb'n'm'*
$\Gamma_{2u}(+-)$			a_z	*Pb'nm*
$\Gamma_{3u}(-+)$			g_z	*Pbn'm*
$\Gamma_{4u}(--)$	a_x	g_y		*Pbnm'*

where $\mathbf{s}_1$, $\mathbf{s}_2$, $\mathbf{s}_3$, and $\mathbf{s}_4$ describe the magnetic moments of the four Nd atoms in the unit cell: $Nd_1(x,y,1/4)$, $Nd_2(-x,-y,3/4)$, $Nd_3(x+1/2,-y+1/2,3/4)$, and $Nd_4(-x+1/2,y+1/2,1/4)$ with $x=0.0108$ and $y=0.0439$. As the *x* and *y* coordinates are not rational numbers, the extinction conditions concern only the (00*l*) reflections (see Table III).

B. Determination of the magnetic structure

For each symmetry-allowed magnetic mode, we checked systematically the agreement between the observed and calculated patterns. The best results were obtained for the $(--c_z)$ mode belonging to the $\Gamma_{1g}(++)$ representation. They are summarized in Table IV and illustrated in Fig. 3. The resulting magnetic structure is shown in Fig. 4. Notice that the existence of nonzero *x* and/or *y* components is symmetry forbidden. In this magnetic arrangement, each Nd^{3+} magnetic moment is coupled antiferromagnetically to the four nearest neighbors in the plane (**a**,**b**) and ferromagnetically with the two nearest neighbors situated above and below this plane. Notice that the present model differs from the one proposed for explaining the specific-heat data (*g* mode), where all the nearest-neighbor interactions were supposed to be antiferromagnetic.[10,20]

The possibility of a magnetic moment arrangement resulting from the mixing of two irreducible representations was also carefully tested. In general, the goodness

TABLE III. Conditions ruling the existence of the (00*l*) magnetic reflections for the *f*, *a*, *g*, and *c* modes.

f	$l=2n$
a	$l=2n+1$
g	Forbidden
c	Forbidden

TABLE IV. Results of the Rietveld refinements for $NdGaO_3$ at 300 mK and 10 mK.

T (mK)	$\mu^{Nd}(\mu_B)$	Pol. (%)	R_{mag}	R_{wp}	R_{exp}	R_{Bragg}
300	1.1(2)	29(16)	18.4	13.1	2.70	7.82
10	1.1(1)	70(9)	12.9	13.3	2.45	7.50

of the fit was worse than in the former case. The only spin configuration which gave similar reliability factors was $(0c_yc_z)=(0c_y-)+(--c_z)$, which is a basis function of a reducible representation of the direct sum $\Gamma_{1g}(--c_z)\oplus\Gamma_{2g}(0c_y-)=\Gamma_{1g}\oplus\Gamma_{2g}(0c_yc_z)$. The value of the c_y component, however, was so small that within the experimental uncertainty imposed by the resolution, we can consider the magnetic structure as described by a pure mode $(--c_z)$.

C. Saturation value and temperature dependence of the Nd^{3+} magnetic moment

The refined value of the electronic magnetic moment of Nd^{3+} at 300 mK is $1.1(2)\mu_B$, far below the single-ion value ($3.27\mu_B$). This reduction is due to crystal-field effects. To see that, we have calculated the saturation magnetic moment from a set of CEF parameters derived from inelastic neutron-scattering measurements. In a previous work,[21] such a set of parameters was derived for $NdGaO_3$ using the geometrical constraints of the noncentrosymmetric space group $Pbn2_1$. However, the correct symmetry is *Pbnm*, which considerably reduces the number of CEF parameters in Eq. (4). We then have reanalyzed the previous neutron data by using the least-squares fitting procedure described in detail in Ref. 21. In a first step, all the fourth- and sixth-order parameters were correlated to B_0^4 and B_0^6, respectively, by taking into account the geometry of the eighth nearest oxygen neighbors [see Eq. (3) in Ref. 21]. In a second step, B_4^4 and the real part of B_4^6 were allowed to vary independently, since their influence on the CEF splitting is rather strong. For the fitting procedure we used seven quantities observed in the neutron spectroscopic measurements (four CEF energies and three intensity ratios) and, in addition, the saturation moment $\mu_{sat}^{Nd^{3+}}=[0,0,1.1(2)\mu_B]$ determined in the present work. Sets of CEF parameters which produced an easy axis of magnetization different from the z axis were discarded in the fitting procedure. Following this procedure, we arrived at a unique set of parameters (see Table V) which reproduce the observed CEF energies and intensities reasonably well (see Table VI). The molecular field constant for $T_N=0.97$ K is $\lambda=0.050$ meV, which yields a saturation moment of $\mu=1.3\mu_B$. The values of the diagonal components of the g tensor calculated from the CEF parameters are $g_x=2.227$, $g_y=2.483$, and $g_z=2.549$.

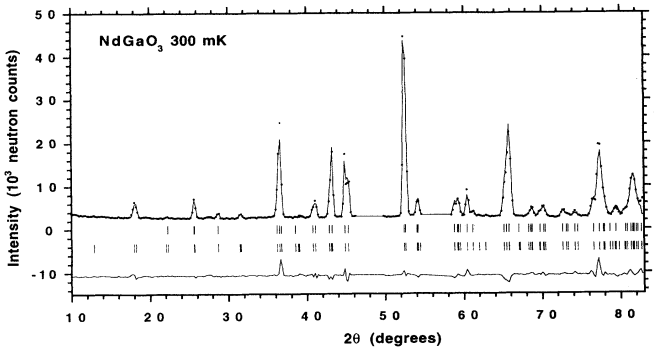

FIG. 3. Observed and calculated neutron-diffraction patterns of $NdGaO_3$ at 300 mK. The points are the raw data. The continuous line is the calculated profile. The upper row of vertical marks indicates the positions of the nuclear (crystallographic) reflections and the lower row those of the magnetic reflections allowed by the mode $(--c_z)$. The measuring time for this pattern was 8 h.

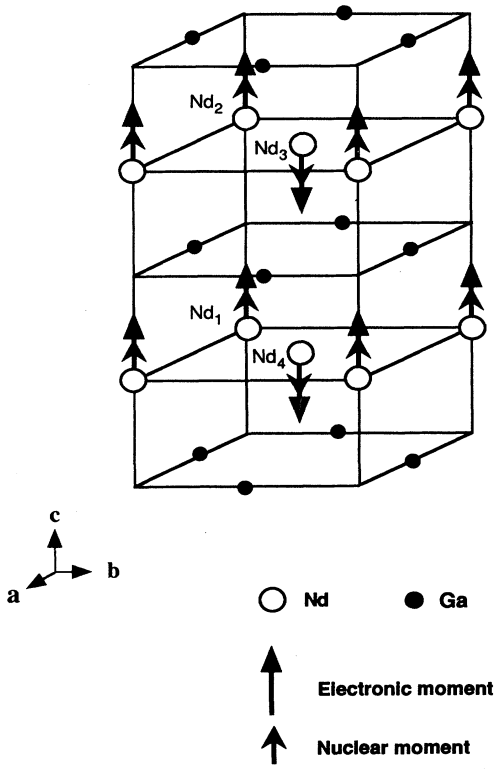

FIG. 4. Magnetic structure of $NdGaO_3$.

The temperature dependence of the Nd^{3+} magnetic

TABLE V. CEF parameters derived for $NdGaO_3$ using the *Pbnm* symmetry. The parameters B_q^k given without errors were correlated to B_0^k.

		B_q^k (meV)	
k	q	Real part	Imaginary part
2	0	49.7±3.0	
2	2	33.2±2.0	51.0±2.0
4	0	−95.1±1.0	
4	2	−16.5	99.8
4	4	−25.6±1.0	−47.9±2.0
6	0	−75.4±3.0	
6	2	18.6	39.1
6	4	−157.6±2.0	−0.29
6	6	24.2	−4.5

TABLE VI. Observed and calculated CEF energy levels and normalized transition probabilities for $NdGaO_3$.

$\Gamma^{(i)}$	E_{obs} (meV)	E_{calc} (meV)	$\lvert\langle\Gamma^{(i)}\rvert J_p \rvert\Gamma^{(1)}\rangle\rvert^2_{obs}$	$\lvert\langle\Gamma^{(i)}\rvert J_p \rvert\Gamma^{(1)}\rangle\rvert^2_{calc}$
$\Gamma^{(1)}$		0		
$\Gamma^{(2)}$	11.4±0.2	11.4	1.0	1.0
$\Gamma^{(3)}$	22.5±0.4	22.5	0.2±0.1	0.3
$\Gamma^{(4)}$	52.7±1.0	52.2	0.9±0.2	0.5
$\Gamma^{(5)}$	68.0±1.0	68.2	0.6±0.2	0.4

moment $\langle m_z \rangle$ is displayed in Fig. 5. The points are the results of the Rietveld refinements. The solid line is the result of a calculation based on the Hamiltonian (3), which is diagonalized in the space spanned by the basis vectors $|m_z, I_z\rangle$ [see Eqs. (6) and (7)] by an iteration procedure until convergence for both $\langle m_z \rangle$ and $\langle I_z \rangle$ is obtained. As the hyperfine constants for ^{143}Nd and ^{145}Nd are slightly different (see Sec. IV), we repeated the iteration procedure for both isotopes, the final value of $\langle I_z \rangle$ being its weighted average (see Sec. VI). Within the experimental accuracy imposed by the smallness of the magnetic moment, the agreement is rather satisfactory.

D. Origin of the magnetic coupling

It was mentioned in the introduction that the most likely mechanisms for the Nd-Nd magnetic coupling are superexchange and the classical dipolar interaction. To decide between both possibilities, we have evaluated the dipolar energy per ion associated to all the symmetry-allowed magnetic configurations listed in Table II (see the Appendix for the details of the calculation). The results are displayed in Table VII. From them, it is clear that the $(00c_z)$ mode is the most stable configuration in the presence of dipolar interactions *alone*. However, the dipolar energy per ion associated to this magnetic mode ($E_d = -2.917$ μeV/ion $= 33.85$ mK/ion), is far below the Néel temperature (970 mK). In consequence, a Nd-Nd interaction based on the dipole-dipole coupling does not seem very likely. The superexchange interaction is then the leading mechanism, in agreement with the conclusions derived from the specific-heat measurements.

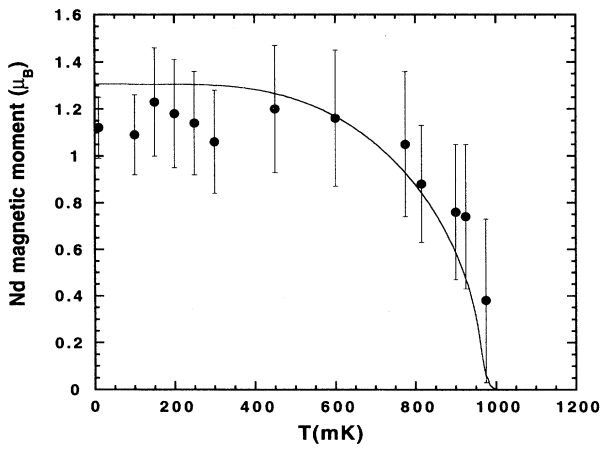

FIG. 5. Temperature dependence of the Nd^{3+} electronic magnetic moment. The points are the results of the Rietveld refinements and the solid line is the mean-field calculation (see text).

VI. NUCLEAR POLARIZATION BELOW 300 mK

The origin of the sudden increase of the magnetic reflections below 300 mK is due to the polarization of the ^{143}Nd and ^{145}Nd nuclear spins in the hyperfine field created by the Nd electronic moments. To arrive at this conclusion, we used the different **Q** dependences of the magnetic and the nuclear cross sections. We used also our knowledge of the sign of the hyperfine constant (negative for both ^{143}Nd and ^{145}Nd), which constrains the nuclear spins to orient themselves parallel to the electronic magnetic moments. If a net nuclear polarization exists, the electronic and the nuclear magnetic moments will show the same type of ordering (c_z mode, see Fig. 4).

Let us first discuss the existence of purely "nuclear"[22] reflections. Since the electronic magnetic scattering is proportional to the component of the magnetic moment normal to the scattering vector, it is straightforward to see that the $(00l)$ reflections will show zero intensity. Such limitation does not occur in the case of the scattering arising from the existence of a net polarization of the

TABLE VII. Dipolar energy per ion associated to each one of the symmetry-allowed magnetic configurations of Table II. Note that for Γ_{2g}, Γ_{3g}, Γ_{1u}, and Γ_{4u}, the magnetic moments can be oriented along one (or two) arbitrary directions in the (**a**,**b**) plane. The magnetic structure is then, in general, noncollinear, the only collinear arrangements occurring when one of the two components (x or y) is zero. In the table, we have calculated the dipolar energy for each of the two collinear arrangements and for the noncollinear magnetic structure which results when the magnetic moments of the Nd_1 ion form an angle of 45° with both the **a** and **b** crystallographic axes.

I.R.	Mode	$E_{dipolar}$/ion (μeV)
Γ_{1g}	$(--c_z)$	−2.917
Γ_{2g}	$(f_x 0-)$	−2.363
	$(0c_y-)$	+1.497
	$(f_x c_y-)$	−0.412
Γ_{3g}	$(c_x 0-)$	+1.419
	$(0f_y-)$	−2.428
	$(c_x f_y-)$	−0.538
Γ_{4g}	$(--f_z)$	−2.321
Γ_{1u}	$(g_x 0-)$	−0.060
	$(0a_y-)$	−2.729
	$(g_x a_y-)$	−1.406
Γ_{2u}	$(--a_z)$	+5.410
Γ_{3u}	$(--g_z)$	−0.113
Γ_{4u}	$(a_x 0-)$	−2.681
	$(0g_y-)$	+0.173
	$(a_x g_y-)$	−1.227

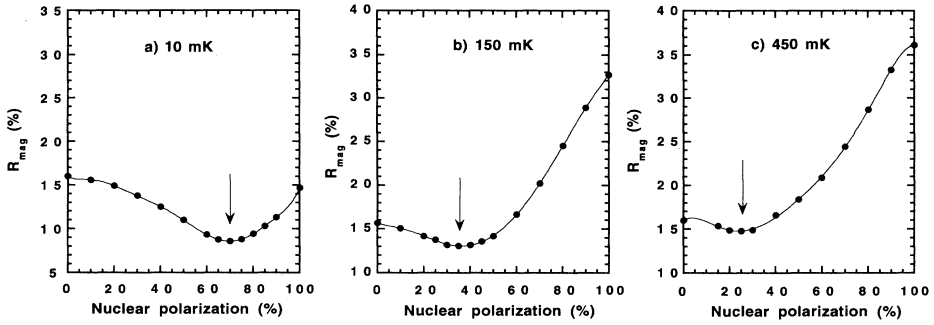

FIG. 6. Variation of the magnetic R factor versus the percentage of nuclear polarization used in the refinement of the neutron powder-diffraction patterns: (a) 10 mK, (b) 150 mK, (c) 450 mK. The solid lines are guides for the eye.

nuclear spins. Then, if the $(00l)$ reflections exist, they will be purely nuclear in origin. Unfortunately, they are forbidden by a c mode (see Table III). In consequence, even in the presence of hyperfine-enhanced nuclear polarization, no extra reflections will appear below 300 mK, and the only effect in the neutron powder-diffraction patterns will be the enhancement of the pre-existent magnetic reflections. This is exactly what we observe in our measurements.

An additional confirmation of the hyperfine-enhanced nuclear origin of the intensity increase observed at low temperature is given by the different dependence of the magnetic form factor $f(\mathbf{Q})$ and the "nuclear" Fermi length b_N with Q (or with the scattering angle 2θ via $Q=4\pi\sin\theta/\lambda$). To evaluate this effect, we added to our Rietveld program a special subroutine containing the three contributions displayed in Eq. (1) which allowed the *simultaneous* refinement of the electronic magnetic moment and the percentage of nuclear polarization.

In Fig. 6(a) we show the variation of the magnetic R factor for the 10 mK neutron-diffraction pattern as a function of the percentage of **P**. The curve has been obtained by fixing the nuclear polarization to a given value (between 0 and 100) and fitting the electronic moment. The minimum is located near 70%, all the other values yielding larger reliability factors. Similar curves have been obtained for the remaining temperatures and from the refinement of both the difference and the full diffraction patterns [see Figs. 6(b) and 6(c)]. The minimum R_{mag} moves towards smaller polarizations by increasing the temperature, in accord with the expected behavior.

The existence of this minimum is a direct consequence of the sensibility of the neutron powder-diffraction patterns to the different **Q** dependences of the magnetic and "nuclear" cross sections. This effect is more clearly shown in Fig. 7, where the observed difference pattern (10 mK−1.4 K) refined by using different restrictions is displayed. In Fig. 7(a), which shows the better reliability factors, we refined simultaneously μ^{Nd} and **P**. The obtained values were, respectively, $1.1(1)\mu_B$ and 70%, in close agreement with those corresponding to the minimum of Fig. 6(a). In Fig. 7(b) we show the same pattern refined by supposing that the reflections are purely magnetic (0% nuclear polarization). Note that, in spite of the larger value obtained for the Nd magnetic moment ($\approx 2\mu_B$), the agreement is not very good, especially at large scattering angles. In Fig. 7(c) we have assumed the nuclear spins to be 100% polarized and the agreement is

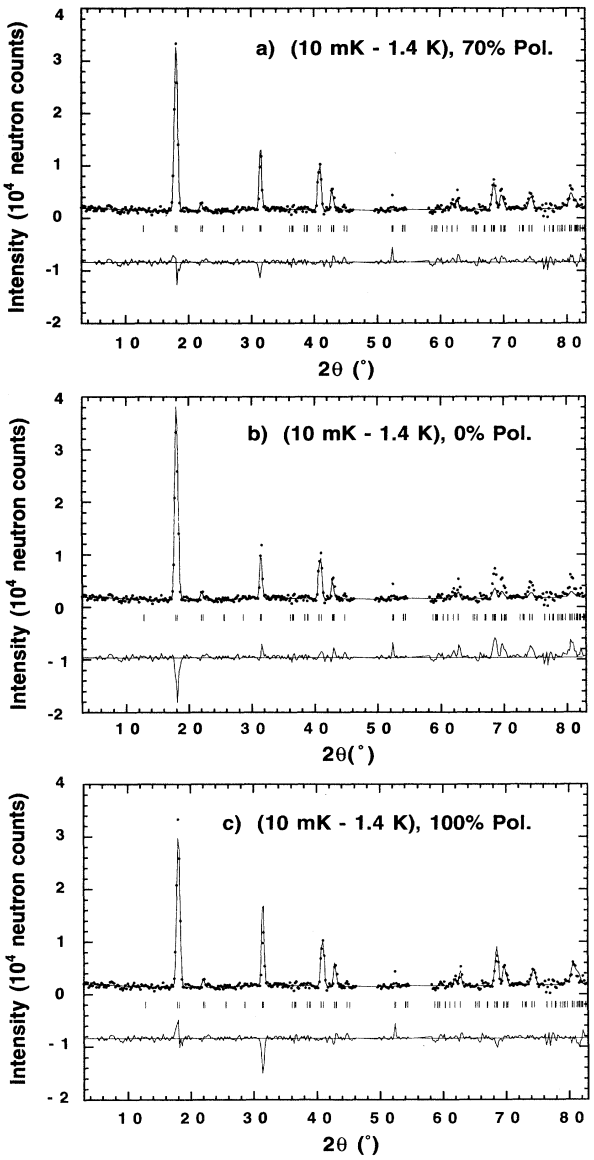

FIG. 7. Observed and calculated difference (10 mK−1.4 K) neutron-diffraction patterns of $NdGaO_3$ normalized to a counting time of 83 h. The points are the raw data. The continuous line is the profile calculated with nuclear polarizations of 70% (a), 0% (b), and 100% (c). The vertical marks indicate the positions of the reflections allowed by the mode $(--c_z)$. Note that for this magnetic arrangement, there are no purely hyperfine-enhanced nuclear reflections.

also worse than in Fig. 7(a).

The experimental and calculated values of the nuclear polarization are shown in Fig. 8. The contributions of the two Nd isotopes are shown separately, together with their weighted average. Taking into account the absence of free parameters in the model (see Sec. IV), in agreement is reasonably good. The discrepancies are probably due to the smallness of the neutron powder-diffraction signal, the relatively large errors of the incoherent Fermi lengths of ^{143}Nd and ^{145}Nd and the utilization of the hyperfine constants measured on diluted Nd^{3+} ions in salts.[1]

As a closing remark, we would like to stress that similar nuclear polarization effects are expected to exist in all the compounds with ordered Nd^{3+} electronic moments. This statement has been nicely verified on materials with very different structural and electronic properties, as for example $NdPd_3$ (cubic, metallic),[3] $NdNiO_3$ (orthorhombic, metal-insulator transition at 200 K),[5] and Nd_2CuO_4 (tetragonal, insulator).[4] An important exception, not yet understood, is the high-T_c superconductor $NdBa_2Cu_3O_7$ (Refs. 23 and 24) where no traces of nuclear polarization have been found down to 10 mK.

VII. CONCLUDING REMARKS

In this study, we have presented an overall picture of the magnetic behavior of $NdGaO_3$ between 10 mK and 1.4 K. By means of neutron powder diffraction we have observed the antiferromagnetic ordering of the Nd^{3+} sublattice below $T_N \approx 1$ K. The magnetic moments are oriented along the c axis in a c_z mode, in contrast to previous predictions.[20] The main contribution to the magnetic Nd-Nd interaction seems to be superexchange, the classical dipole-dipole interaction being too small to account for the observed Néel temperature. The saturation value of the Nd^{3+} magnetic moments is $\approx 1.1\mu_B$ in good agreement with the CEF calculations.

Concerning the *XY* behavior proposed for this system,[10] the values of the components of the *g* tensor along the three crystallographic axes obtained in Sec. V C suggest a much more isotropic behavior ($g_x \approx g_y \approx g_z$). Thus, in spite of the good description of the macroscopic data provided by the *XY* model ($g_z \ll g_{xy}$),[10] it does not seem to be very appropriate for the understanding of the magnetic properties of $NdGaO_3$ on a microscopic level.

Below 300 mK, a strong enhancement of the magnetic reflections has been observed. The different **Q** dependence of the "nuclear" and magnetic cross sections allowed us to interpret this increase as being due to the hyperfine-enhanced polarization of the ^{143}Nd and ^{145}Nd nuclear moments. Its temperature dependence agrees with the calculation performed by using the hyperfine constants of these isotopes reported in the literature.

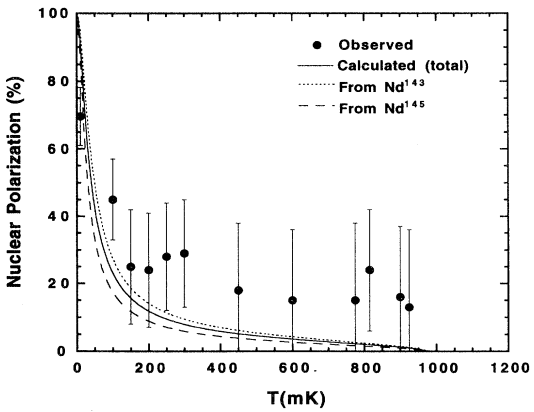

FIG. 8. Temperature dependence of the polarization of the ^{143}Nd and ^{145}Nd nuclear spins. The points are the results of the Rietveld refinements and the solid line is the calculation described in the text.

ACKNOWLEDGMENTS

Financial support by the Swiss National Science Foundation and the European Community is gratefully acknowledged. The authors would like also to thank S. Fischer for expert assistance in the preparation and operation of the dilution refrigerator and J. Rodríguez-Carvajal for his help in the calculation of the dipolar energy.

APPENDIX: DIPOLAR ENERGY CALCULATIONS

For the evaluation of the dipolar energy we followed the method described by Bertaut.[25,26] In this procedure, the well-known formula for the interaction energy per ion

$$E_d = \frac{1}{2N} \sum_{i,j,i\neq j} \frac{3(\boldsymbol{\mu}_i \cdot \hat{\mathbf{r}}_{ij})(\boldsymbol{\mu}_j \cdot \hat{\mathbf{r}}_{ij}) - (\boldsymbol{\mu}_i \cdot \boldsymbol{\mu}_j)}{r_{ij}^3} \tag{A1}$$

is substituted by the equivalent expression

$$E_d = \frac{2\pi}{3nV_c} \left\{ \sum_{\mathbf{h}} (3|\mathbf{h} - D(\mathbf{h})|^2 - h^2 |D(\mathbf{h})|^2) \frac{\varphi(\mathbf{h})}{h^2} - \left| \sum_j^n \boldsymbol{\mu}_j \right|^2 \right\} . \tag{A2}$$

Here, $\boldsymbol{\mu}_i$ and $\boldsymbol{\mu}_j$ are the magnetic moments of the ions situated in the positions $\mathbf{r}_i$ and $\mathbf{r}_j$, $\mathbf{r}_{ij} = \mathbf{r}_j - \mathbf{r}_i$, $\hat{\mathbf{r}}_{ij} = \mathbf{r}_{ij}/r_{ij}$, $\mathbf{h}$ is a reciprocal space vector, N is the number of magnetic

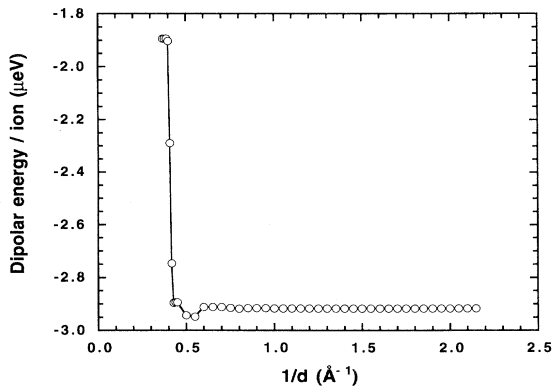

FIG. 9. Dependence of the dipolar energy per Nd ion as a function of the maximum radius $1/d = |\mathbf{h}|$ used in expression (A2).

ions in the crystal, and V_c and n are the volume and the number of magnetic ions of the magnetic unit cell, respectively. $D(\mathbf{h})$ is the dipolar factor, defined as

$$|D(\mathbf{h})| = \sum_j^n \boldsymbol{\mu}_j \exp(2\pi i \mathbf{h}\mathbf{r}_j) \quad \text{(A3)}$$

and $\varphi(\mathbf{h})$ is the Fourier transform of a function $f(\mathbf{r})$ chosen such as to be nonzero in a sphere of radius R_0 ($2R_0$ is the smallest distance between two magnetic atoms), and zero for $r > R_0$. In our case, we have chosen $f(\mathbf{r}) = 15(1+2x^3-3x^2)/(4\pi R^2)$ with $x = r/R_0$.

Expressions (A1) and (A2) differ in the sense that the summation is made in the real and the reciprocal spaces, respectively. From the point of view of the calculation, the latter procedure is more advantageous. The reason is that, while the standard expression (A1) is the summation of an oscillating, slowly convergent series, Eq. (A2) is the difference of two positive quantities with good convergence properties.

Figure 9 shows the variation of the dipolar energy per ion as a function of the radius of the reciprocal sphere which contains the points used in the summation. The magnetic moment arrangement used in the calculation is that of Fig. 4 (c_z mode) with $\mu^{Nd} = 1.1\mu_B$ and the structural parameters of Table I. Notice that the convergence is reached for $1/d \approx 0.6$ Å^{-1} (220 reciprocal points). Similar curves have been obtained for the remaining symmetry-allowed configurations, the convergence being reached in all the cases for $1/d < 1$ Å^{-1}.

The values of E_d for the modes of Table II are displayed in Table VII. The lowest dipolar energy corresponds to the magnetic structure experimentally observed (-2.917 μeV/ion). The less stable configuration is the a_z mode, with $E_d = +4.471$ μeV. The g modes proposed in Refs. 10 and 20 are also found to be less favorable than the c_z arrangement.

[1]B. Bleaney, *Proceedings of the Third Quantum Electronics Conference* (Dunod, Paris, 1964).

[2]H. Glättli and M. Goldman, in *Methods of Experimental Physics*, edited by K. Sköld and D. L. Price (Academic, New York, 1987), Vol. 23, Pt. C.

[3]O. Elsenhans, P. Fischer, A. Furrer, K. N. Clausen, H. J. Purwins, and F. Hulliger, Z. Phys. B **82**, 61 (1991).

[4]T. Chattopadhyay and K. Siemensmeyer, Europhys. Lett. **29**, 579 (1995).

[5]S. Rosenkranz *et al.* (unpublished).

[6]W. Marti, P. Fischer, F. Altorfer, H. J. Scheel, and M. Tadin, J. Phys. Condens. Matter **6**, 127 (1994).

[7]H. Brusset, Bull. Soc. Chem. France **8**, 2886 (1967).

[8]W. Marti, J. P. Rivera, F. Kubel, H. J. Scheel, and H. Schmid, Ferroelectrics (to be published).

[9]W. Marti (unpublished).

[10]F. Bartolomé, M. D. Kuz'min, R. I. Merino, and J. Bartolomé, IEEE Trans. Magn. **30**, 960 (1994).

[11]J. Schefer, P. Fischer, H. Heer, A. Isacson, M. Koch, and R. Thut, Nucl. Instrum. Methods Phys. Res. Sect. A **288**, 477 (1990).

[12]J. Rodríguez-Carvajal, Physica B **192**, 55 (1993).

[13]M. Steiner, L. Bevaart, Y. Ajiro, A. J. Millhouse, K. Ohlhoff, G. Rahn, H. Dachs, U. Scheer, and B. Wanklyn, J. Phys. C **14**, L597 (1981).

[14]B. Roessli, P. Fischer, U. Staub, M. Zolliker, and A. Furrer, Europhys. Lett. **23**, 511 (1993).

[15]P. J. Brown, J. B. Forsyth, P. C. Hansen, M. J. M. Leask, R. C. C. Ward, and M. R. Wells, J. Phys. Condens. Matter **2**, 4471 (1990).

[16]A. Abragam and B. Bleaney, *Electron Paramagnetic Resonance of Transition Ions* (Clarendon, Oxford, 1970).

[17]B. G. Wybourne, *Spectroscopic Properties of Rare Earths* (Interscience, New York, 1965).

[18]C. W. Nielson and G. F. Koster, *Spectroscopic Coefficients for the p^n, d^n and f^n Configurations* (MIT, Cambridge, MA, 1964).

[19]F. Bertaut, Acta Crystallogr. A **24**, 217 (1968).

[20]F. Bartolomé, M. D. Kuz'min, J. Bartolomé, J. Blasco, J. García, and F. Sapiña, Solid State Commun. **91**, 177 (1994).

[21]A. Podlesnyak, S. Rosenkranz, F. Fauth, W. Marti, A. Furrer, A. Mirmelstein, and H. J. Scheel, J. Phys. Condens. Matter **5**, 8973 (1993).

[22]The term "nuclear," commonly used for the scattering of neutrons by the ions's nuclei [b_c^2 term in formula (1)] serves here to designate the scattering arising from the existence of a net polarization of the nuclear spins [$\frac{1}{2}b_N^2 I^2 + \frac{1}{2}\alpha b_N \mathbf{M}_\perp^* \mathbf{I} + \frac{1}{2}\alpha b_N \mathbf{M}_\perp \mathbf{I}^*$ terms in formula (1)].

[23]P. Fischer, B. Schmid, P. Brüesch, F. Stucki, and P. Unternährer, Z. Phys. B **74**, 183 (1989).

[24]K. N. Yang, J. M. Ferreira, B. W. Lee, M. B. Maple, W.-H. Li, J. W. Lynn, and R. W. Erwin, Phys. Rev. B **40**, 10963 (1989).

[25]F. Bertaut, J. Phys. Radium **13**, 499 (1952).

[26]F. Bertaut, J. Phys. (Paris) **39**, 1331 (1978).